Green Chemistry

PAPER

View Article Online
View Journal | View Issue

Cite this: *Green Chem.*, 2026, **28**, 945

Sustainable phosphate-catalyzed synthesis of non-symmetric pyrazines in water – mechanistic insights, biocatalytic applications and industrial potential†

Jorge González-Rodríguez, [a,b] Valentina Jurkaš, [a,c] Eva Puchľová,[d] Maren Podewitz, [e] Fabio Parmeggiani, [f] Margit Winkler, [a,c] Peter Both,[d] Peter Šiška[d] and Florian Rudroff *[b]

Received 11th September 2025,
Accepted 19th November 2025

DOI: 10.1039/d5gc04772b

rsc.li/greenchem

Pyrazines are pivotal flavor compounds with widespread applications in the food, pharmaceutical, and chemical industries. Their natural abundance is low, and traditional synthetic methods often involve hazardous conditions unsuitable for the food sector. In this study, we present a novel biocatalytic methodology for synthesising non-symmetric trisubstituted pyrazines using aminoacetone dimerisation followed by electrophile incorporation under environmentally benign conditions, catalyzed by phosphate anion. The approach includes the employment of L-threonine dehydrogenase from *Cupriavidus necator* to generate aminoacetone *in situ* from natural L-threonine, integrating biocatalysis with green chemistry principles. Detailed mechanistic investigations, supported by control experiments and DFT calculations, revealed the critical role of phosphate buffering, an E1cB elimination, and a tautomerisation-driven pathway for product formation. The methodology demonstrates broad substrate scope and scalability, yielding pyrazines with diverse structural modifications up to 96% yields. This work establishes a starting point for the industrial production of non-symmetric pyrazines, addressing current regulatory and environmental demands in the flavor and fragrance sector.

Green foundation

1. This work presents a very mild and "natural" method for the synthesis of non-symmetric pyrazines, which represents a high-end class of fragrance and flavour compounds.
2. We investigated the synthesis of non-symmetric pyrazines in water under the catalysis of phosphate anions at slightly elevated temperatures. We elucidated the mechanism of the reaction and its substrate scope. So far, non-symmetric alkylpyrazines have not been synthesised in a purely natural way on a preparative scale (25 mM, up to 90% yield). Finally, we developed a chemo-enzymatic cascade (threonine dehydrogenase), starting from L-threonine, for the synthesis of the high-value flavour compound 2-ethyl-3,6-dimethyl pyrazine.
3. Our research can be improved by process optimisation for the chemo-enzymatic cascade starting from the renewable amino acid L-threonine. The enzyme Thr-dehydrogenase could be engineered towards better performance, improved stability and higher solvent tolerance.

Introduction

Pyrazines, volatile nitrogen-containing heterocyclic compounds, are widely distributed in plants,[1,2] insects,[3,4] fungi, and bacteria,[5,6] serving as odor signals to repel predators and protect vegetation.[7] Non-symmetric pyrazines, with diverse applications in pesticides, dyes, and pharmaceuticals,[8–10] are extracted from natural sources and employed to enhance flavors in various processed foods and beverages such as coffee, cocoa, meat, and potato-products. In this sense, there is a growing demand for sustainability in industries, particularly in the food sector, driven by daily consumption and

[a]*Austrian Centre of Industrial Biotechnology (ACIB), Krenngasse 37/2, 8010 Graz, Austria*
[b]*Institute of Applied Synthetic Chemistry, TU Wien, Getreidemarkt 9/163-OC, 1060 Wien, Austria. E-mail: florian.rudroff@tuwien.ac.at*
[c]*Institute of Molecular Biotechnology, TU Graz, Petersgasse 14, 8010 Graz, Austria*
[d]*Axxence Slovakia s.r.o., Mickiewiczova 9, 81107 Bratislava, Slovakia*
[e]*Institute of Materials Chemistry, TU Wien, Getreidemarkt 9/165, 1060 Wien, Austria*
[f]*Dipartimento di Chimica, Materiali ed Ingegneria Chimica "Giulio Natta", Politecnico di Milano, Piazza Leonardo Da Vinci 32, 20133 Milan, Italy*

†We would like to dedicate this work to Prof. Iván Lavandera, a good friend and valuable colleague who passed away way too early. This work perfectly suits his interests, which were at the border between chemistry and biocatalysis.

healthy eating. The flavor and fragrance industry has experienced significant growth, with global market size tripling since the early 21st century. This surge is primarily motivated by global demands for flavor and aroma-enhanced food production, spurred by consumer preferences and technological advancements that qualify products to be labelled as natural. Specifically, the European (European Food and Safety Regulation, EFSA) as well as the American (Food and Drug Administration, FDA) regulation on flavors (EEC No 1334/2008) defines natural flavoring substances as those obtained through appropriate physical, enzymatic, or microbiological processes from material of vegetable, animal, or microbiological origin, either in their raw state or after processing for human consumption using traditional food preparation methods.[11] However, as of now, there are no registered biotechnological syntheses for the industrial production of pyrazine derivatives declared as natural. Consequently, extraction from natural sources remains the sole means of accessing pyrazines for this purpose. Nonetheless, their low natural abundance in sources like sugar beet molasses (0.01 wt%) has driven the search for more effective production methods.[11] In this sense, traditional synthetic methods, although efficient, often involve hazardous conditions unsuitable for the food industry,[12,13] prompting efforts to develop procedures using components from natural origins. Biocatalytic approaches have emerged as dominant in this regard, offering the ability to operate under aqueous and mild conditions, aligning with the criteria for natural processes. Consequently, numerous research groups have endeavored to devise a standardised methodology capable of facilitating the transition of the industry from extraction techniques to enzyme-based syntheses. Different fermentative and biocatalytic approaches, either employing living cells or isolated proteins have been developed. Pyrazines are ubiquitously distributed in many microorganisms,[14–16] and some of them have been employed to produce pyrazines, although with very limited success.[17–19] Usually, low product titers, complex pyrazine mixtures, and difficulties in isolations were encountered.

At first glance, the synthesis of pyrazines is simply based on the condensation of either diketones with diamines or the self-condensation of α-aminoketones. Based on this, Turner and co-workers developed a biocatalytic protocol employing amino transaminases for the generation of the aminoketone precursor *in situ*, although only symmetric pyrazines could be attained in moderate yields, and an amine donor was required (Fig. 1).[20] Kroutil and co-workers published a series of papers in which the discovery of a new reactivity of ene-reductases led to the formation of pyrazines.[21,22] However, only symmetrical and heavily substituted pyrazines can be accessed through this approach.

The methodologies that have come closer to the goal are hybrid approaches combining biocatalysis and organic synthesis. Peng *et al.* proposed the microbial synthesis of acetoin in very high titers, which could then be subjected to treatment with different ammonium salts at 100 °C to generate ligustrazine (tetramethylpyrazine).[23] Also, very recently, Walker and co-workers proposed the employment of carboligases to synthesise suitable α-hydroxyketones, which, after treatment with 1,2-diamines and KOH in diethyl ether, would yield mixtures of the highly pursued short-chain non-symmetric alkyl pyrazines.[24] To the best of our knowledge, there was no methodology available which only employed "natural" reagents for the synthesis of these scaffolds in an non-symmetric manner until the ground-

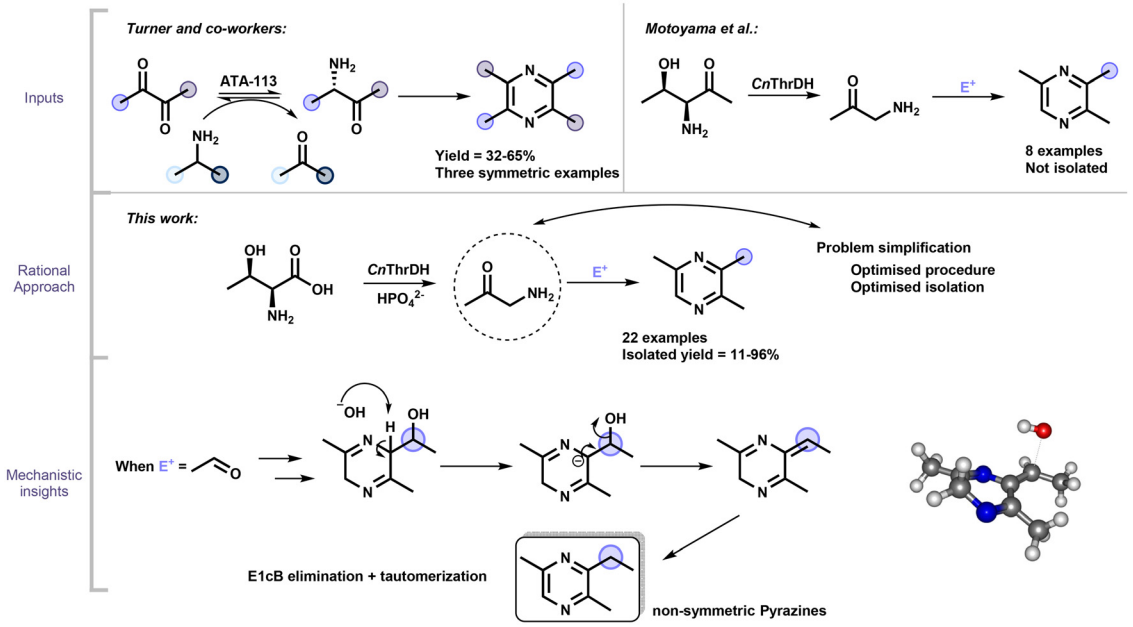

Fig. 1 Overview of the biobased synthesis of pyrazines. In this work, starting from the simple starting material α-aminoacetone we gained an understanding of the transformation, thus leading to enhanced results that were further rationalised through control experiments and DFT calculations.

breaking work of Motoyama *et al.* combining L-threonine dehydrogenases and aldehydes was published in 2021 (Fig. 1).[25] In this research, based on a putative mechanism proposed by Adams *et al.* for the production of these compounds through the Maillard reaction in 2008,[26] they were able to capture the dihydropyrazines intermediates with alkyl aldehydes to obtain non-symmetrically substituted pyrazines. The yields were very low, and the products could not be isolated.

In this work, we describe the synthesis of multiple non-symmetric trisubstituted pyrazines through aminoketone dimerisation followed by the incorporation of electrophiles under natural and environmentally friendly conditions. In contrast to previous works, we managed to isolate all the compounds in moderate to good yields, building the foundations for a possible future incorporation into an industrial setup. Subsequently, we coupled this methodology with L-threonine dehydrogenase from *Cupriavidus necator* to generate the aminoacetone precursor *in situ* from natural and inexpensive L-threonine.[27] Throughout this investigation, phosphate participation was identified and proven to facilitate the transformation. A detailed mechanism for this reaction is presented, supported by control experiments and computational studies, paving the way for future optimisation and the design of efficient synthesis strategies for these valuable compounds.

Results and discussion

Selective synthesis of di- and trisubstituted pyrazines

Non-symmetrically substituted pyrazines create signature perceptions in foods and beverages and are also significant due to their pharmacological properties.[28,29] In the quest for an efficient synthesis and isolation of these scaffolds, we hypothesised that the preparation of trisubstituted pyrazines *via* aminoacetone **1a** dimerisation, followed by the incorporation of an electrophile under biocompatible conditions could be achieved in a single-step manner. Thus, we selected acetaldehyde **2a** as our model electrophile due to its simplicity, availability and compatibility with biocatalytic setups and, subsequently, the reaction was carried out under standard conditions: 4 eq. of **2a**, phosphate buffer 100 mM at pH 9, 50 °C, and a reaction time of 2 hours at a substrate concentration of 25 mM, which led to an impressive 81% GC yield. Although we expected some conversion conducting the reaction under completely aqueous conditions, the outcome exceeded expectations. Further optimisation, such as varying the temperature within biocompatible ranges (20–60 °C), increasing reaction times or changing substrate and/or electrophile concentrations, did not improve the previous result, although we could reduce the concentration of electrophile from 4 to 3 eq. (for further details see Table S1). Due to the need to work within the food industry regulations, no cosolvents were studied in this optimisation.

Next, we tested a diverse array of electrophiles to assess the generality of the protocol (Fig. 2). As a result, we successfully synthesised several aliphatic pyrazines using this methodology, including both linear (**3a**, **c–d**) and cyclic (**3e**) variants, as well as 2,5-dimethylpyrazine without the addition of any electrophile (**3b**). To address the synthesis of **3c**, which gave the lowest yield of aliphatic aldehydes, we experimented with both aqueous formaldehyde (40% w/w, stabilised with 15% MeOH, *i.e.* formalin) and paraformaldehyde **2b**.

While the former yielded only 8%, **2b** enabled the isolation of **3c** in a modest yet appreciable yield (20%). We believe that the reason for this behavior could be the higher degree of hydration of formaldehyde, rendering it unreactive towards nucleophilic attack. Following this, a plethora of aromatic aldehydes underwent screening, yielding trisubstituted pyrazines. Benzaldehyde **2e**, when utilised as a reaction partner, yielded product **3f** with a 59% yield. Subsequently, both electron-donating (**3g–h**) and electron-withdrawing (**3i–m**) substituents on the phenyl ring were explored. In both scenarios, the desired pyrazines were, in general, isolated in moderate yields.

The reactivity of derivatives with substituents in different positions of the aromatic ring was studied as well. The *para* position seemed to be the most favoured one for the reaction to occur (**3i**), while the *meta* substitution led to a substantially lowered yield of 32% (**3j**). However, the *ortho* derivative could only be isolated in a very low yield. Substitutions in this position seem to be unsuitable (see SI for further information). The observation is in accordance with the mechanism we postulated and the results we observed for other derivatives, as the steric hindrance is the most influential parameter for this reaction to take place.

As anticipated, however, a higher proportion of **3b** was observed in instances where electron-rich benzaldehydes **2f–g** were employed. This occurrence can be attributed to the favored reaction with oxygen over the intended pathway, owing to the lower electrophilicity of these substrates (Fig. 3a, Pathway B). Conversely, heteroaromatic aldehydes such as furan-3-carboxaldehyde **2m** and thiophene-3-carboxaldehyde **2n** emerged as excellent coupling partners, likely due to their lower steric demands.

Consequently, the corresponding pyrazines **3n** and **3o** were obtained with yields of 96% and 69%, respectively. When we attempted to employ alkynes as Michael acceptors, we were delighted to observe that but-3-yn-2-one **2o** and methyl propiolate **2p** produced the corresponding pyrazines **3p** and **3q** with yields of 41% and 67%, respectively. The lower yield obtained for the ketone derivative is mostly attributed to side reactions. We were also interested in testing the amide derivative propiolamide **2v**, but no product was formed. To investigate if the free amide could be hampering the reactivity, we synthesised *N*,*N*-dimethylpropiolamide **2q** and subjected it to the optimised reaction conditions, leading to a 19% yield. Finally, we tested functionalised aldehydes as electrophiles for this transformation. Thus, we selected methylglyoxal **2r**, which would yield a complementary carbonyl compound to **3p**, and citronellal **2s**. Satisfyingly, we were able to isolate both products, **3s** with a yield of 11% and **3t** in 47% yield. To delineate the boundaries of the developed protocol, we also investigated the reactivity of ketones as reagents. However, in the case of acetone **2t**, a side reaction occurred, depleting the starting

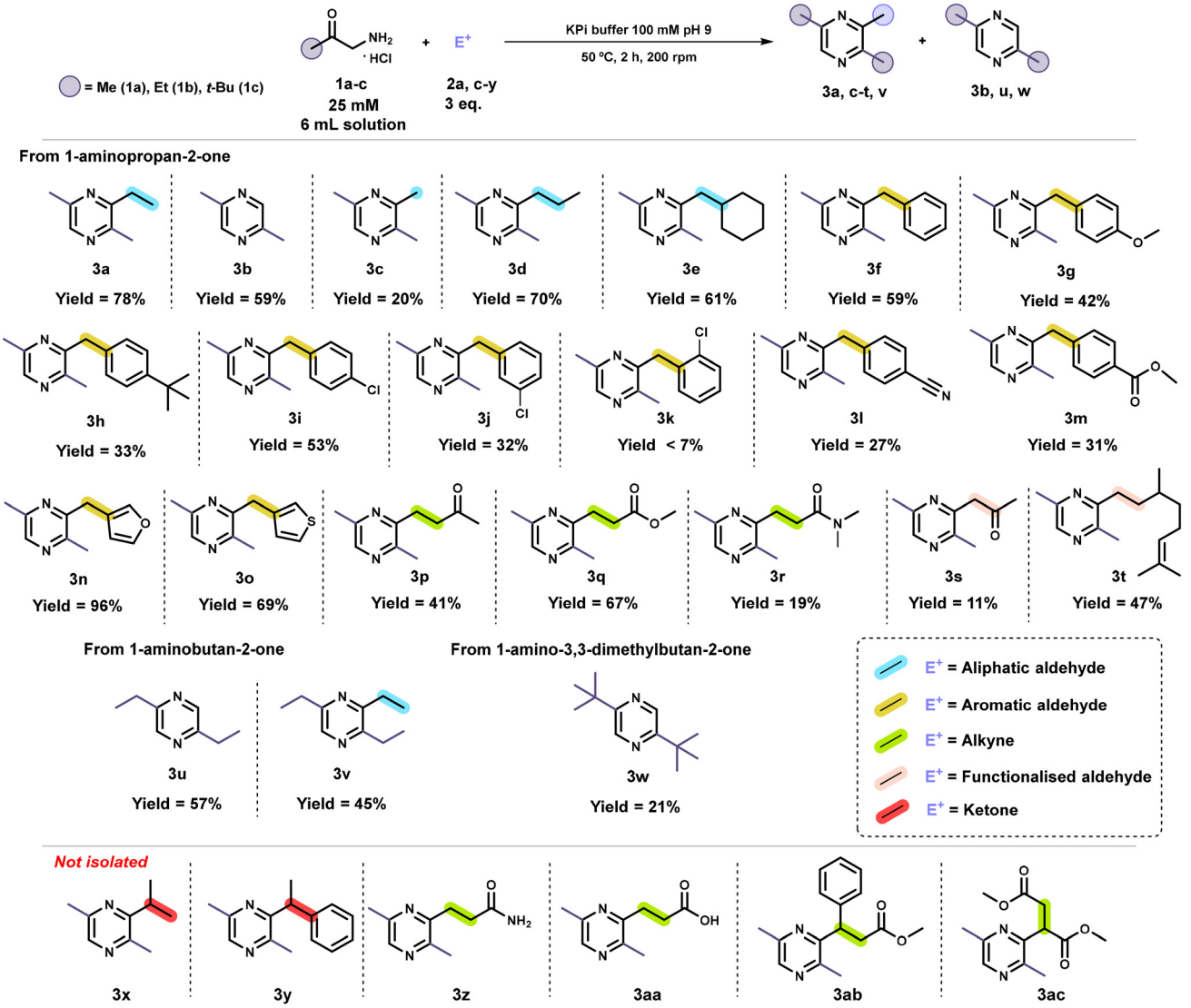

Fig. 2 Scope of the pyrazine formation reaction. By simplifying the approach and starting from aminoketones, a broad substrate scope could be accessed, greatly varying the nature of the electrophiles employed, yielding the different target pyrazines in moderate to good isolated yields. The position and nature of the electrophiles is represented by colors. When no color is indicated, it means that no electrophile was added to the reaction.

material. When acetophenone **2u** was employed, 2,5-dimethylpyrazine **3b** was isolated along with the starting ketone, reflecting the less electrophilic character of ketones. Propiolic acid **2w** did not yield the desired pyrazine **3aa** when employed as a Michael acceptor, while methyl phenylpropiolate **2x** exhibited no reactivity, likely due to steric hindrance and/or excessive electron density, rendering it unreactive toward nucleophilic attack by the species described in this contribution. To define this behaviour more precisely, we explored dimethyl but-2-ynedioate **2z** as a highly deactivated alkyne, but no product **3ac** could be observed, demonstrating that only acetylenes are accepted as electrophiles for this protocol. To conclude the scope of our study, we explored the reactivity of two different starting materials. When 1-aminobutan-2-one hydrochloride **1b** was utilised without an electrophile, smooth dimerisation occurred, resulting in the formation of 2,5-diethylpyrazine **3u** with a 57% isolated yield. Encouragingly, we observed that the addition of acetaldehyde **2a** was also well tolerated, allowing us to isolate the corresponding pyrazine **3v** with a yield of 45%. Finally, when 1-amino-3,3-dimethylbutan-2-one hydrochloride **1c** was subjected to the same conditions, no product formation was expected due to the higher steric hindrance and lower electrophilicity of the carbonyl scaffold. However, we were surprised to isolate compound **3w** with a low but remarkable yield of 21%.

Mechanistic investigations

After optimising the reaction conditions and broadening the substrate scope, we recognised the importance of investigating the underlying mechanism, given the high value of the pro-

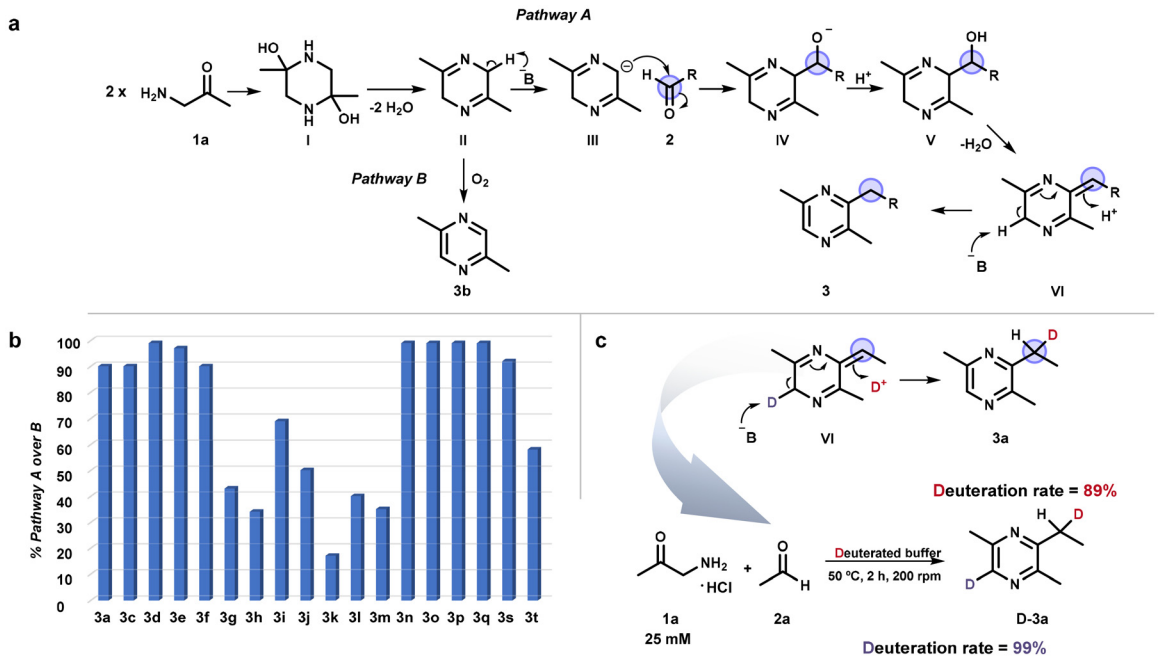

Fig. 3 Mechanistic investigations. (a) Mechanistic proposal adapted from Adams *et al.*,[26] used as a benchmark for this study, featuring the two possible reaction pathways of the transformation. Molecular oxygen triggers autooxidation of intermediate **II**, leading to the depletion of the substrate through the formation of pyrazine **3b**. (b) Relationship between pathways A and B for each substrate of the scope, depicted as a percentage of pathway A. (c) Deuteration experiment under optimised conditions.

ducts obtained through this process. The proposed mechanistic framework is derived from the work of Adams *et al.*,[26] and is illustrated in Fig. 3a. After the dimerisation of aminoketone **1a**, dihydropyrazine **II** is formed. With regard to Pathway A, this intermediate might be deprotonated by a base in the reaction media, rendering it nucleophilic enough to attack an electrophile, in the case of the example, an aldehyde. The alcohol **IV**, formed after protonation with water, could be dehydrated, rendering the unsaturated derivative **V**, which would aromatise to yield the desired pyrazine **3**. As can be observed, Pathway B is competing with Pathway A through autooxidation by aerial oxygen of the dihydropyrazine intermediate to yield **3b**. To determine the extent of this competition between pathways A and B, we measured the **3**/**3b** ratio of each reaction, which is shown in Fig. 3b (see section V in the SI file for detailed ratios). To improve reaction yields and investigate this behavior further, we reproduced the example involving paraformaldehyde under oxygen-free conditions and measured the yield using GC to avoid introducing the volatility variable. The ratio of **3c**/**3b** increased from 90/10 to >99/1, indicating the absence of oxygen hindered the autooxidation reaction. Hence, we selected candidates with nearly 50/50 ratios—citronellal derivative **3t** (58/42) and anisaldehyde derivative **3g** (43/57)—and tested them under oxygen-free conditions. Selectivity improved significantly: **3t** reached 83/17 with a yield increase from 47% to 58%, while **3g** reached 61/39 with the same yield. These results confirm the hypothesis of competing pathways A and B (Fig. 3a). Next, to prove the tautomerisation step (Fig. 3a, **VI**), we let the reaction between **1a** and acetaldehyde **2a** occur in deuterated phosphate buffer, adjusted to pH 9 with sodium deuteroxide, expecting major deuteration in the secondary carbon of the side chain (Fig. 3c). We were glad to observe an 89% incorporation of deuterium, thus pointing again towards our hypothesis. A 99% incorporation was also detected in the only possible position of the aromatic ring, which is in accordance with how highly labile those protons are in α position, between the amine and the carbonyl scaffold in the starting material **1a**. To demonstrate further that the recovery of aromaticity and, therefore, tautomerisation is the driving force for the incorporation of the electrophile (Fig. 3a, VI), we designed two different experiments, which are depicted in Fig. 4. In the first, methyl acrylate **2z** (A) and methyl propiolate **2p** (B) were studied as electrophiles. As we hypothesised, when example A was followed, there were not enough electrons in the system for it to be able to aromatise through tautomerisation. Therefore, the autooxidation pathway (Fig. 3a, Pathway B) was favoured and only starting material **1a** and **3b** were recovered. However, when methyl propiolate **2p** was employed, the molecule had enough electrons to rearrange towards aromatic pyrazine, thus yielding **3q** with a remarkable 67% yield. Secondly, we tried to reproduce this same philosophy this time employing iodomethane **2aa** and diiodomethane **2ab** as electrophiles (Fig. 4b). In this second case, the employment of **2aa** (A) leads to an intermediate that possesses no other leaving group, rendering it unable to gain aromaticity. However, when diiodomethane **2ab** was employed (B), yields comparable to the ones obtained with formaldehyde in solution (8%) were achieved, which demonstrates again the need for the dihydro-

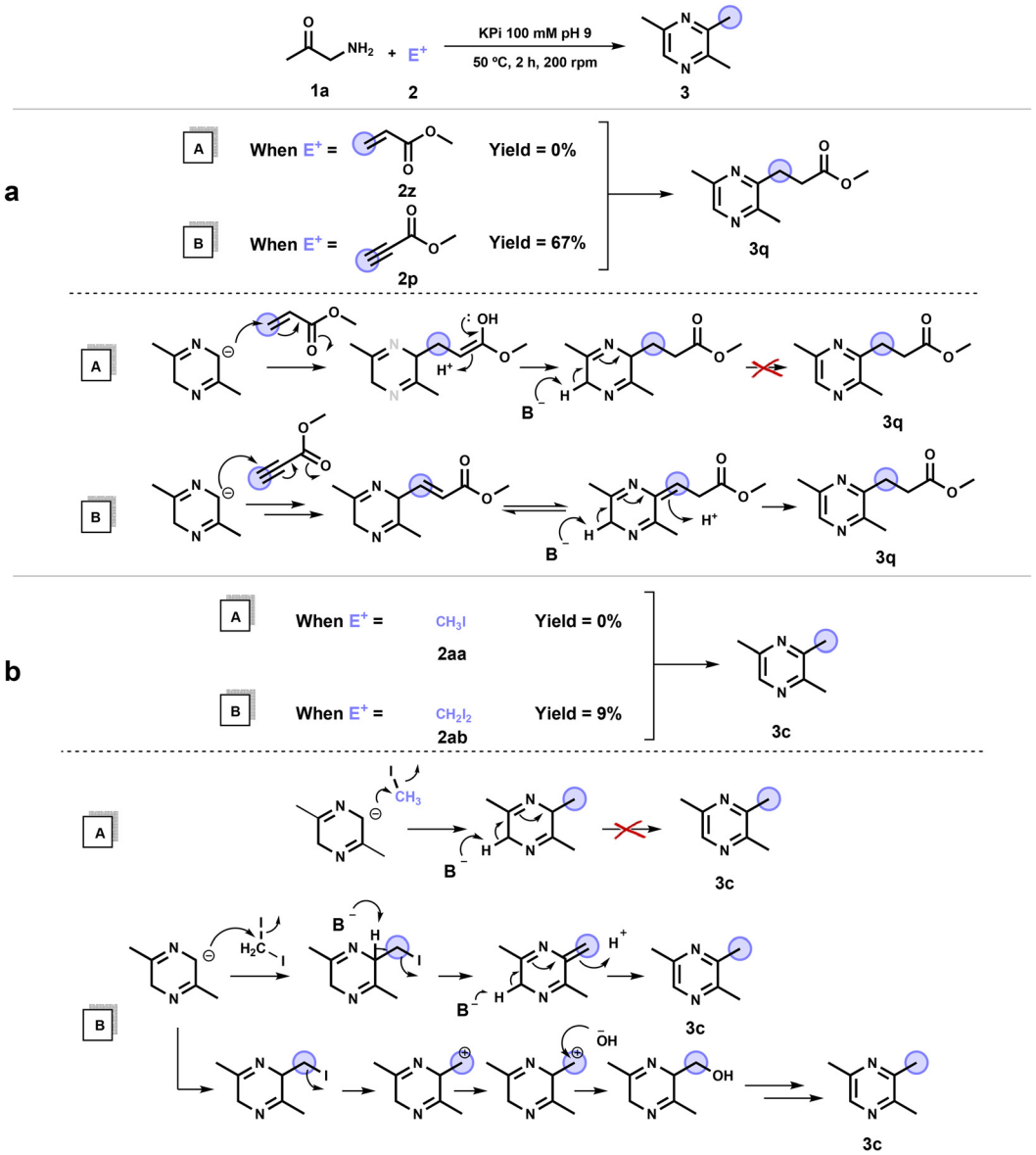

Fig. 4 Tautomerisation experiments. The aromatic character of the final pyrazine product is critical to drive the equilibria towards the products and make the incorporation of the electrophile predominate over the oxidation pathway. Therefore, experiments with methyl acrylate **2z**, methyl propiolate **2p**, iodomethane **2aa** and diiodomethane **2ab** were carried out to reveal this effect and prove that a tautomerisation step is necessary. This hypothesis is further supported by the deuteration experiments shown in Fig. 3c. The position of the electrophile is represented by the blue circle.

pyrazine intermediate to recover aromaticity, which we propose to be the driving force of the reaction, also in accordance with the deuteration experiment (Fig. 3c).

We next sought to further investigate the necessary conditions for the dimerisation reaction to occur (Table 1). We first conducted the reaction in carbonate buffer and water at pH 9, to check how phosphate influences the reaction (Table 1, entries 1–3). We were surprised to observe how important it was for this transformation to succeed. When carbonate was employed, the yield decreased to 42% (Table 1, entry 2) and preparing water at pH 9 employing the minimum amount required of NaOH led to a poor yield of 9% (Table 1, entry 3).

These results strongly indicate that phosphate and a finely adjusted pH are minimum requirements for this reaction, and also that the present salts should be promoting the reaction rather than only buffering the system. To improve the solubility of the substrate and, hypothesising that water might not be necessary for the transformation and could even hinder it, given that two dehydration steps are involved, we tried to carry out the transformation employing several organic solvents, namely MeOH, THF and CPME (Table 1, entries 4–6) but almost no conversion to any pyrazine could be observed.

As a further proof of phosphate catalyzing this reaction, we explored microaqueous reaction system (MARS) conditions,[30]

Table 1 Testing of different media in **3a** synthesis

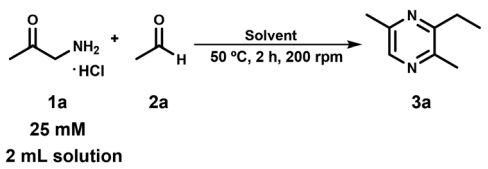

Entry	Solvent	Yield **3a** [a] (%)	pH
1	KP_i buffer pH 9	81	7.5
2	Carbonate buffer pH 9.5	42	7.8
3	Water (pH 9)[b]	9	2
4	MeOH	<1	n.a.
5	THF	2	n.a.
6	CPME	3	n.a.
7	CPME[c]	36	n.a.

[a] Yields determined by GC analysis with external calibration. [b] Adjusted with NaOH. [c] Reaction carried out in CPME adding 10 μL of KP_i buffer 100 mM pH 9. n.a. not applicable.

by using CPME with only 10 μL KP_i buffer 100 mM pH 9, and the result was an astonishing 36% yield (Table 2, entry 7).

In order to rationalise these results, and considering that aminoacetone was added as a hydrochloride salt, we measured the pH in aqueous samples of the crude mixtures after the reaction was completed. We observed a significant drop in pH (Table 1, entries 1–3), which explains the lack of reactivity in pure water. However, the huge difference between carbonate and phosphate was still not clear. We attribute this behavior to the consumption of aminoacetone in the reaction medium, which decreases the amount of base present. This trend can also be observed in the Knorr pyrrole reaction.[31] With these results in hand, we hypothesised that phosphate could carry out a reactivity similar to that of a traditional BINOL-phosphate derived catalyst in which several functional groups can be activated employing this anion (Fig. 5).[32] This process consists of the HOMO raising of a nucleophile or the LUMO lowering of an electrophile through hydrogen bonding between the different parts of the phosphate molecule. Such activation can occur in different manners: mono, dual, and bifunctional activation. In our specific case, as the resulting pH is 7.5, the predominant species in solution is expected to be the hydrogen phosphate anion[33] which may carry out the three types of activation depicted in Fig. 5.

During these experiments, we detected a byproduct in the reaction, which we identified as 5-ethyl-3,6-dimethyl-2-(1-hydroxyethyl)pyrazine **4a** (Table 2), that was obtained after a double deprotonation between intermediates **III–V** (Fig. 3a, Pathway A). The formation of **4a** from **3a** was ruled out by incubating **3a** at the optimal conditions for 24 h, isolating it unaltered.

To further rationalise the buffer influence as well as the formation of this byproduct, we studied different conditions, as described in Table 2. In this table, we observe the crucial role of the buffer in the reaction. By selecting anions with similar properties to phosphate, such as HEPES and MOPS (Table 2, entries 2 and 3), we noted that the reaction proceeds with higher yields compared to when carbonate is used (Table 1, entry 2), likely due to a similar effect as when phosphate is employed. An interesting observation is that with these two buffer systems, the byproduct ratio decreases significantly, suggesting an activation effect occurring between intermediates **III–V** (Fig. 3a, Pathway A). Lower pH resulted in lower yields and *vice versa*. However, the byproduct ratios were not significantly affected. Increasing buffer capacity to 200 mM rendered the products in similar yields than before (Table 2, entry 6). Finally, we reduced the buffer concentration to improve the environmental impact of the transformation. However, insufficient buffer capacity resulted in significantly lower yields (Table 2, entries 7–9). Interestingly, this also led to

Table 2 Effect of different buffers in the obtention of **3a** and **4a**

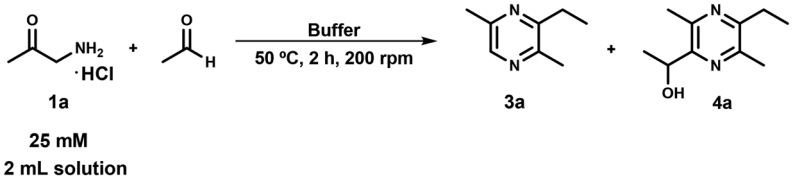

Entry	Buffer	Buffer conc. (mM)	Buffer pH	Reaction pH	GC yield **3a** [a] (%)	**3a**/**4a**
1	KP_i	100	8	7.3	80	81/19
2	HEPES	100	8	7.3	72	98/2
3	MOPS	100	8	7.3	66	98/2
4	KP_i	100	7	6	65	80/20
5	KP_i	100	9	7.5	81	80/20
6	KP_i	200	8	7.9	78	82/18
7	KP_i	10	8	4	24	96/4
8[b]	KP_i	10	8	4	29	96/4
9	KP_i	25	8	5	28	92/8
10	KP_i	50	8	5.7	41	88/12

[a] Yields determined by GC analysis with external calibration. [b] Reaction carried out for 12 hours.

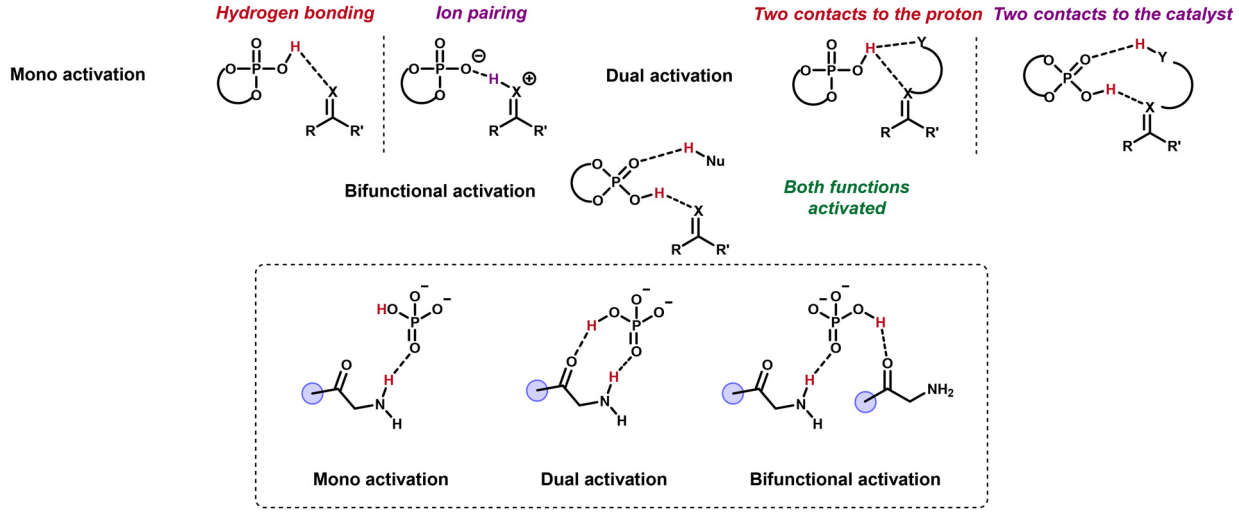

Fig. 5 BINOL-phosphate catalysis types of activation. Figure adapted from Rueping and co-workers[32] depicting the different types of phosphate-mediated activations. In the box, a hypothetical visual description of how this effect could take part in the transformation described in this manuscript.

a lower **3a**/**4a** ratio, strengthening the hypothesis of the catalysis occurring in one of the steps between **III** and **VI** (Fig. 3a, Pathway A).

To further investigate these results, we carried out autotitration experiments keeping the pH constant (pH 8). Even though the yield employing pure water was higher (40%), again highlighting the importance of pH for this transformation, the yield using KP_i buffer under the same conditions was 22% higher (see SI, section V.4 for further details). In addition, HEPES, water and KP_i showed different side-product profiles. As further proof, we carried out these autotitration experiments employing different concentrations of KP_i, 100 mM, 10 mM and 1 mM. In all cases, the yield increased in a significant manner indicating a catalytic mechanism.

These facts together serve as a final proof of the buffer effect in the system. In order to figure out where and how this phenomenon could be taking place and elucidate the complete mechanism, we conducted DFT calculations which will be discussed in the next section.

Quantum chemical investigations

After discovering buffer intervention in our system, we conducted extensive DFT calculations to validate our findings. These calculations also serve as a valuable tool for refining or developing future methodologies for non-symmetric pyrazine synthesis. Combined with our experimental data, we investigated the pyrazine formation process, which, to our knowledge, had not been elucidated before. We first considered the formation of the non-symmetric pyrazine starting from specie **II** (Fig. 6). The first step (**II–III**), a hydroxyl-mediated proton abstraction, shows a very low barrier of 16.1 kJ mol^{-1}, which is consistent with how electron-poor the dihydropyrazine **II** is and its antiaromatic character. Interestingly, the nucleophilic attack from specie **III** to acetaldehyde also showed a very low barrier (**III–IV**, 14.8 kJ mol^{-1}). This might not be intuitive at first, but matches the experimental results regarding the competing pathways A and B (Fig. 3a). As the **3a**/**3b** ratio is 90/10, the energetic barrier has to be quite low to overcome the autoxidation with molecular oxygen. The protonation step **IV–V** has no barrier in the electronic surface, so we assumed that it is very low. Next, the most favorable development was the deprotonation of the substituted carbon (**V–VI**), showing an energetic barrier of 18.7 kJ mol^{-1}, which was followed by a hydroxyl elimination step **VI–VII**, the rate-limiting step of the reaction, with an activation energy of 91.0 kJ mol^{-1}, which is consistent with our experimental data. These two steps describe a traditional E1cB mechanism which was expected due to our reaction conditions (protic media and a poor leaving group). This elimination was confirmed, contrasting it with E1- and E2-type eliminations, which modeling showed to be unviable. The final tautomerisation step (**VII-2**) is barrierless, as expected for a rearomatisation, and we believe it acts as a thermodynamic well which drives the reaction equilibrium forward. This tautomerisation step has been also proven experimentally through deuteration experiments and employment of different electrophiles (Fig. 3b and 4). In the search for the role of hydrogen phosphate, we turned our attention towards the formation of dimer **I** (Fig. 3a). When we first simulated this step of the mechanism just using hydroxyl anions as a base, the energy barrier obtained was low, (49.8 kJ mol^{-1}), indicating that the reaction should be feasible, although the need for a slightly basic pH discards the possibility of running it in pure water (Table 1). Next, we modeled this step with hydrogen phosphate as a potential catalyst, considering all possible scenarios outlined in Fig. 5. Optimisations of all reactants consistently converged toward the dual activation case (Fig. 5, lower box), which we selected as our starting point. We then calculated the HOMO–LUMO gap for two models—one with a protonated

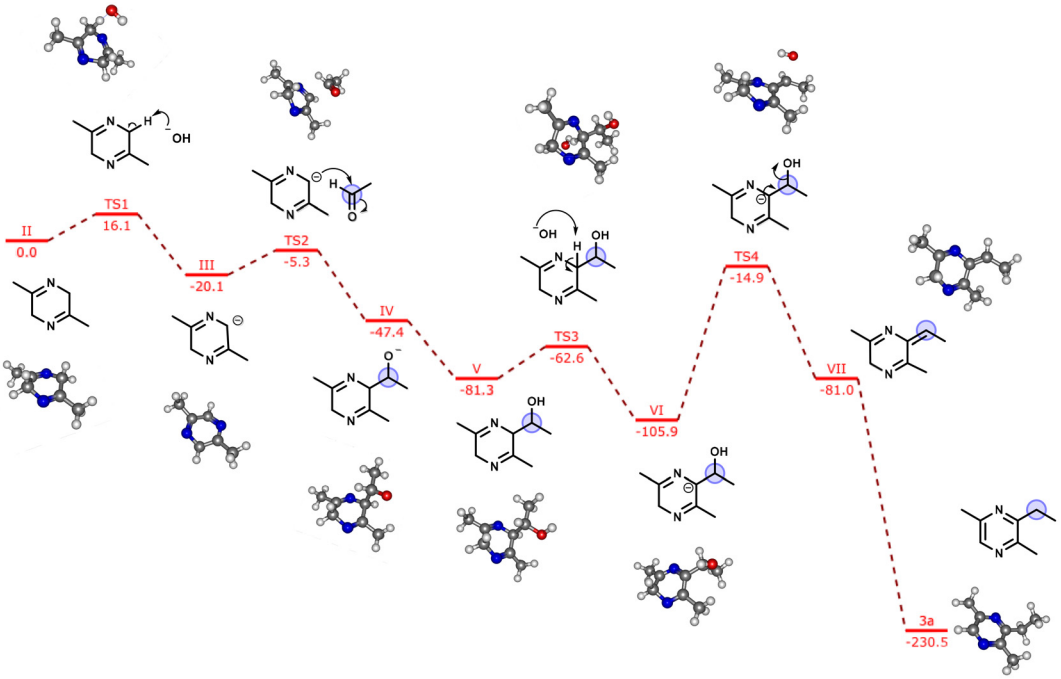

Fig. 6 Free energy reaction profile describing the formation of non-symmetric pyrazines. The DFT calculations have been carried out employing ωB97x-D4/def2-TZVP in implicit water, described by conductor-like polarisable continuum model (CPCM). To obtain free energies (given in kJ mol^{-1}) thermodynamic corrections have been added at 323.15 K, which is the temperature of the reaction. Explicit solvent molecules (water) have been added in cases in which the species modelled need stabilisation.

amine moiety and one unprotonated—both of which were low enough to suggest potential activation in this dimerisation step. However, attempts to model the transition states for both cases proved unviable, making catalysis in this initial step less likely. Next, we attempted to model the case of activation of intermediate **VI** with hydrogen phosphate through hydrogen bonding, which would lower the energetic barrier of the hydroxyl elimination (Fig. 6). Firstly, we analised the HOMO–LUMO gaps of the species involved, which were qualitatively lowered with regard to the same step without any activation.

However, our calculations did not yield a converged transition state in these cases, so we could not demonstrate the hydrogen phoshate catalysis neither in this step.

Nevertheless, the experimental results strongly indicate the involvement of salts in the reaction. This discrepancy suggests that additional investigation is needed to better understand their role and underlying mechanism. Finally, although previous studies carried out with this type of molecules supported the dimerisation of aminoketones towards pyrazines, we decided to model ourselves the formation of intermediate **II**.[34] According to our calculations, the process should be energetically favored with an overall free energy of −125.8 kJ mol^{-1} (see section VI in the SI file for further details).

A biocatalytic cascade for the synthesis of pyrazines

With the reactivity of the system established and the mechanism elucidated, we turned our attention to developing a biocatalytic process for the *in situ* generation of the key intermediate, aminoacetone **1a**. We selected L-threonine dehydrogenase from *Cupriavidus necator*[27] (*Cn*ThrDH) and evaluated its performance in the model reaction with acetaldehyde **2a** as the electrophile. Under the initial reaction setup—10 mg lyophilised cell-free extract (CFE), 25 mM L-Thr in 100 mM KP_i (pH 8), 4 equivalents of **2a**, and 1 equivalent of NAD^+ at 40 °C for 16 h—the product **3a** was obtained in 59% yield (Table 3, entry 1), outperforming previously reported systems.[25] Control experiments confirmed that both *Cn*ThrDH and NAD^+ were essential for the observed transformation (Table 3, entries 2 and 3). We then sought to increase the supply of **1a** by increasing the L-Thr concentration, while proportionally increasing the amount of **2a** and NAD^+. However, this led to a substantial reduction in product formation (Table 3, entry 4), suggesting enzyme inhibition. To counteract this, we increased the reaction temperature to 50 °C and reduced the concentration of **2a** to alleviate aldehyde-induced enzyme deactivation.[35] Notably, decreasing **2a** to 2 equivalents—matching its concentration in the initial reaction setup—restored the yield of **3a** to 29% (Table 3, entry 7), indicating this level may approximate the enzyme's tolerance limit for the electrophile. In parallel, we reverted the NAD^+ loading to that used in the initial reaction setup, which improved catalytic performance and led to a 52% yield of **3a** (Table 3, entry 8). Interestingly, the total amount of pyrazine products (**3a** + **3b**) reached 68%, exceeding the theoretical maximum yield based on the NAD^+ stoichiometry (50%) and suggesting partial NAD^+ regeneration by components of the crude extract. Further decreasing **2a** to equimolar amounts

Table 3 Optimisation of the biocatalytic cascade towards trisubstituted pyrazine

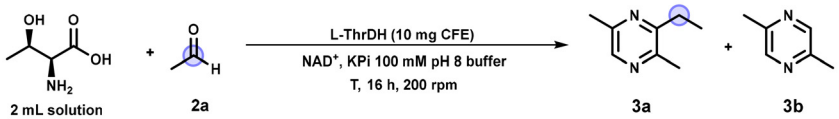

Entry	**2a** (eq.)	L-Thr (mM)	Enzyme	NAD^+ (eq.)	*T* (°C)	**3a** [a] (%)	**3b** [a] (%)
1	4	25	*Cn*ThrDH	1	40	59	<1
2	4	25	Blank	1	40	<1	<1
3	4	25	*Cn*ThrDH	—	40	<1	<1
4	4	50	*Cn*ThrDH	1	40	<1	<1
5	4	50	*Cn*ThrDH	1	50	8	<1
6	3	50	*Cn*ThrDH	1	50	18	<1
7	2	50	*Cn*ThrDH	1	50	29	<1
8	**2**	**50**	***Cn*ThrDH**	**0.5**	**50**	**52**	**16**
9	1	50	*Cn*ThrDH	0.5	50	38	37

[a] Yields determined by GC analysis through external calibration.

increased the total pyrazine yield to 75%, though with an equimolar distribution of **3a** and the disubstituted product **3b** (Table 3, entry 9), underscoring the effect of electrophile concentration on product distribution and chemoselectivity.

To test the generality of the process, we selected two representative electrophiles, benzaldehyde **2f** and furan-3-carboxaldehyde **2k** and subjected them to the optimised conditions described in entry 8, yielding the corresponding trisubstituted pyrazines **3f** and **3l** in 43% and 77% yields, respectively.

Experimental

Selective synthesis of di- and trisubstituted pyrazines 3a–u

The corresponding aminoketone 1 (25 mM) and the desired electrophile 2 (75 mM) were dissolved in 6 mL of KP_i 100 mM buffer, pH 9, in a closed 30 mL glass vial, and the solution was shaken for 2 h at 50 °C in an orbital shaker at 200 rpm. After this time, the mixture was extracted with AcOEt (2 × 6 mL) or Et_2O (2 × 6 mL) depending on the volatility and solubility of the compound. The combined organic layers were dried over Na_2SO_4, filtered, and purified through SiO_2 flash column chromatography employing mixtures of pentane : Et_2O or pentane : AcOEt. The only exception was cyclohexanecarboxaldehyde derivative **3e**, which was found to be unstable when treated with SiO_2. For this example, reverse phase flash column chromatography was carried out employing a Büchi Pure C-850 FlashPrep equipped with a Waters Atlantis C-18 preparative column, using mixtures of water and acetonitrile under neutral conditions. Afterwards, the desired product **3e** was extracted employing AcOEt (3 × 10 mL) dried over Na_2SO_4 and filtered. ^{1}H-NMR, ^{13}C-NMR, and Mass spectroscopy have been carried out for every compound and compared with the ones previously reported in literature (for further details, see SI, section V).

Experiments under oxygen-free conditions

The corresponding aminoketone **1** (25 mM) and the desired electrophile **2** (75 mM) were dissolved in 6 mL of KP_i 100 mM buffer pH 9, previously degassed through cycles of vacuum and argon, followed by bubbling of argon through the solution for 10 minutes. The buffer was transferred to the vials under an inert atmosphere employing a cannula. Then, the reaction was stirred for 2 h at 50 °C in an orbital shaker at 200 rpm. After this time, the mixture was extracted with AcOEt (2 × 6 mL) or Et_2O (2 × 6 mL) depending on the volatility and solubility of the compound. The combined organic layers were dried over Na_2SO_4 and injected directly in the GC for quantification of the products. Employment of ketones **2r** and **2s** under these conditions, to force the nucleophilic addition, did not yield detectable amounts of product (for further details, see SI, section VI).

Deuteration experiments

Aminoketone **1a** (25 mM) and acetaldehyde **2a** (75 mM) were dissolved in 6 mL of deuterated KP_i 100 mM buffer, pH 9, in a closed 30 mL glass vial, and the solution was shaken for 2 h at 50 °C in an orbital shaker at 200 rpm. After this time, the mixture was extracted with deuterated chloroform (2 × 6 mL). The combined organic layers were dried over Na_2SO_4, filtered and analysed through ^{1}H-NMR spectroscopy.

Autotitration experiments

Aminoacetone **1a** (25 mM) and acetaldehyde **2a** were added (75 mM) to the autotitrator dissolved in KP_i buffer (100, 10 or 1 mM), HEPES 100 mM or NaOH 10 mM (pH 8) to a total reaction volume of 30 mL and incubated for 2 h at 50 °C in a plastic, non-air-tight beaker with 30% stirring at a Mettler Toledo T50 autotitrator. For experiments with lower phosphate concentrations (10, 1, and 0 mM KP_i), sodium hydroxide (10 mM) was added to the buffer to maintain the starting pH close to 8.0 The pH was kept at 8.0 with NaOH (0.2 M) (for further details, see SI, section VI).

Computational methodology

Computations in the present study were performed with the ORCA 5.0 utilising the local high performance computing

infrastructure. Electronic ground state calculations, including geometry optimisations, frequencies, and transition-state searches, were carried out with density functional theory (DFT) utilising ORCA and the ωB97x hybrid GGA functional together with Grimme's D4 dispersion correction and Ahlrichs' def2-TZVP basis set. Gibbs free energies at 323.15 K were calculated using the rigid-rotor harmonic oscillator approximation as implemented in ORCA. For geometry optimisations and single-point calculations, implicit solvation was included *via* the CPCM model and water as solvent. Transition States (TSs) were localised with the help of the nudged elastic band method as implemented in the ORCA and confirmed to be first-order saddle points by analysis of the Hessian. Intrinsic reaction coordinate calculations have been employed to verify the correct assignment of TSs by following the eigenvector of the corresponding imaginary frequency, starting from the TS structures and connecting to reactants and products. Optimised structures were visualised with ChemCraft (for further details, see SI, section VII).

Biocatalytic synthesis of pyrazine 3a

L-Threonine (50 mM), NAD^+ (0.5 mM) and the desired electrophile (2.5 eq., 125 mM) were dissolved in 6 mL of KP_i 100 mM buffer, pH 8, in a 30 mL glass vial. Then, 10 mg of *Cn*ThrDH lyophilised CFE was added, the vial was closed, and the solution was shaken for 16 h at 50 °C in an orbital shaker at 200 rpm. After this time, the mixture was extracted with Et_2O (2 × 6 mL). The combined organic layers were dried over Na_2SO_4, filtered, and purified through SiO_2 flash column chromatography employing mixtures of pentane : Et_2O (for further details, see SI, section IX).

Conclusions

This study establishes a mechanistically grounded platform for synthesising non-symmetric pyrazines through aminoketone dimerisation and electrophilic trapping. By systematically exploring substrate scope, we obtained di- and trisubstituted pyrazines (*e.g.*, **3a–3u**) in 20–96% isolated yields using diverse electrophiles, including aliphatic/aromatic aldehydes, alkynes, and functionalised carbonyl compounds. Key to success was optimising aqueous phosphate buffer conditions (pH 9, 50 °C), which suppressed autooxidation while enabling efficient trapping of dihydropyrazine intermediates. DFT calculations and control experiments revealed three critical steps in the mechanism: first, the E1cB elimination of water from the aminoketone dimer ($\Delta G^{\ddagger}$ = 18.3 kcal mol^{-1}) generates a conjugated enamine intermediate; second, tautomerisation to a nucleophilic dihydropyrazine species (**II** in Fig. 3a) occurs, potentially stabilised by phosphate buffer through hydrogen-bonding interactions; and third, electrophilic trapping proceeds *via* competing pathways, where Pathway A involves Michael addition to aldehydes or alkynes and is favored under oxygen-free conditions, while Pathway B leads to autooxidation forming symmetric pyrazines and dominates with electron-rich electrophiles. Oxygen exclusion increases selectivity for Pathway A by 1.4 to 2.3 times in challenging cases (for example, the **3q** product ratio changes from 58/42 to 83/17 relative to **3**/**3b**). Experimental validation confirmed the role of phosphate as a stabiliser for transition states and hypothesised the necessity of the buffer for achieving high yields.

Coupling this chemistry with L-threonine dehydrogenase enabled a fully biocatalytic cascade from renewable L-threonine to flavor-relevant pyrazines. The tandem system operates under aqueous, ambient conditions (25 °C, pH 7.5), aligning with EU/FDA "natural" labeling requirements while bypassing hazardous reagents. This work provides both a synthetic toolbox for non-symmetric pyrazines and a mechanistic framework for optimising similar biocatalytic-electrophilic cascades in heterocycle synthesis.

Author contributions

The manuscript was written through the contributions of all authors. All authors approved the final version of the manuscript. The experimental work was done by JG and VJ. The research was conceived by FR and MW.

Conflicts of interest

There are no conflicts to declare.

Data availability

Additional data can be found in the supplementary information (SI) which was submitted additionally and is publicly available.

Supplementary information is available. See DOI: https://doi.org/10.1039/d5gc04772b.

Acknowledgements

We thank the COMET center acib: Next Generation Bioproduction is funded by BMK, BMDW, SFG, Standortagentur Tirol, Government of Lower Austria, and Vienna Business Agency in the framework of COMET – Competence Centers for Excellent Technologies. The COMET-Funding Program is managed by the Austrian Research Promotion Agency FFG. This work was supported by the Slovak Research and Development Agency under the contract number APVV-20-0317.

References

1 K. E. Murray and F. B. Whitfield, *J. Sci. Food Agric.*, 1975, **26**, 973–986.

2 S. Shinkaruk, M. Floch, A. Prida, P. Darriet and A. Pons, *J. Agric. Food Chem.*, 2019, **67**, 10137–10144.
3 B. P. Moore, W. V. Brown and M. Rothschild, *Chemoecology*, 1990, **1**, 43–51.
4 E. A. Silva-Junior, A. C. Ruzzini, C. R. Paludo, F. S. Nascimento, C. R. Currie, J. Clardy and M. T. Pupo, *Sci. Rep.*, 2018, **8**, 2595.
5 T. Nawrath, J. S. Dickschat, B. Kunze and S. Schulz, *Chem. Biodivers.*, 2010, **7**, 2129–2144.
6 S. Kim, P. F. Hillman, J. Y. Lee, J. Lee, J. Lee, S.-S. Cha, D.-C. Oh, S.-J. Nam and W. Fenical, *J. Antibiot.*, 2022, **75**, 619–625.
7 T. Guilford, C. Nicol, M. Rothschild and B. P. Moore, *Biol. J. Linn. Soc.*, 1987, **31**, 113–128.
8 P. Miniyar, P. Murumkar, P. Patil, M. Barmade and K. Bothara, *Mini-Rev. Med. Chem.*, 2013, **13**, 1607–1625.
9 M. Dolezal and J. Zitko, *Expert Opin. Ther. Pat.*, 2015, **25**, 33–47.
10 Q. Sun and P. Sever, *J. Renin-Angiotensin-Aldosterone Syst.*, 2020, **21**, 147032032097589.
11 F. B. Mortzfeld, C. Hashem, K. Vranková, M. Winkler and F. Rudroff, *Biotechnol. J.*, 2020, **15**, 2000064.
12 P. Daw, A. Kumar, N. A. Espinosa-Jalapa, Y. Diskin-Posner, Y. Ben-David and D. Milstein, *ACS Catal.*, 2018, **8**, 7734–7741.
13 H. Tsurugi, M. Matsuno, T. Kawakami and K. Mashima, *Eur. J. Org. Chem.*, 2022, e202200862.
14 K. S. Rajini, P. Aparna, Ch. Sasikala and Ch. V. Ramana, *Crit. Rev. Microbiol.*, 2011, **37**, 99–112.
15 P. Li, X. Gan, L. Luo and B. Du, *Ann. Microbiol.*, 2017, **67**, 391–393.
16 J. S. Dickschat, H. Reichenbach, I. Wagner-Döbler and S. Schulz, *Eur. J. Org. Chem.*, 2005, 4141–4153.
17 J. S. Dickschat, S. Wickel, C. J. Bolten, T. Nawrath, S. Schulz and C. Wittmann, *Eur. J. Org. Chem.*, 2010, 2687–2695.
18 C. Yang, Y. Xu, K. Xu, G. Tan and X. Yu, *Tetrahedron Lett.*, 2018, **59**, 3084–3087.
19 S. Masuo, Y. Tsuda, T. Namai, H. Minakawa, R. Shigemoto and N. Takaya, *ChemBioChem*, 2020, **21**, 353–359.
20 J. Xu, A. P. Green and N. J. Turner, *Angew. Chem., Int. Ed.*, 2018, **57**, 16760–16763.
21 S. Velikogne, W. B. Breukelaar, F. Hamm, R. A. Glabonjat and W. Kroutil, *ACS Catal.*, 2020, **10**, 13377–13382.
22 W. B. Breukelaar, N. Polidori, A. Singh, B. Daniel, S. M. Glueck, K. Gruber and W. Kroutil, *ACS Catal.*, 2023, **13**, 2610–2618.
23 H. Jiang, Y. Liu, K. Peng, D. Guo, Q. Lou, X. Lu, J. Cheng, J. Qiao, L. Lu and T. Cai, *ACS Synth. Biol.*, 2020, **9**, 2902–2908.
24 G. Attanayake, G. Mao and K. D. Walker, *J. Agric. Food Chem.*, 2021, **69**, 15314–15324.
25 T. Motoyama, S. Nakano, F. Hasebe, R. Miyata, S. Kumazawa, N. Miyoshi and S. Ito, *Commun. Chem.*, 2021, **4**, 108.
26 A. Adams, V. Polizzi, M. van Boekel and N. De Kimpe, *J. Agric. Food Chem.*, 2008, **56**, 2147–2153.
27 T. Ueatrongchit and Y. Asano, *Anal. Biochem.*, 2011, **410**, 44–56.
28 J. Zou, P. Gao, X. Hao, H. Xu, P. Zhan and X. Liu, *Eur. J. Med. Chem.*, 2018, **147**, 150–162.
29 Y. Hu, A. Wang, J. Chen and H. Chen, *Clin. Exp. Obstet. Gynecol.*, 2023, **50**, 164.
30 R. Oeggl, T. Maßmann, A. Jupke and D. Rother, *ACS Sustainable Chem. Eng.*, 2018, **6**, 11819–11826.
31 B. Ashley, A. Baslé, M. Sajjad, A. el Ashram, P. Kelis, J. Marles-Wright and D. J. Campopiano, *ACS Sustainable Chem. Eng.*, 2023, **11**, 7997–8002.
32 D. Parmar, E. Sugiono, S. Raja and M. Rueping, *Chem. Rev.*, 2014, **114**, 9047–9153.
33 K. J. Powell, P. L. Brown, R. H. Byrne, T. Gajda, G. Hefter, S. Sjöberg and H. Wanner, *Pure Appl. Chem.*, 2005, **77**, 739–800.
34 M. A. H. Shipar, *Food Chem.*, 2006, **98**, 403–415.
35 B. Franken, T. Eggert, K. E. Jaeger and M. Pohl, *BMC Biochem.*, 2011, **12**, 10.

